prelim

Xiaoning Wang

March 31, 2021

1 Introduction

1.1 Quark Gluon Plamsa

One of the main purposes of performing the ultra-relativistic heavy ion collisions, such as those done at the Large Hadron Collider (LHC) and the Relativistic Heavy Ion Collider (RHIC), is to produce a hot, dense nuclear matter at extreme temperature and density. Under such conditions, composite states of particles from the nuclei known as hadrons (protons, neutrons, etc.) undergo important phase transitions and dissolve into their constituent particles, quarks and gluons, giving the name for this special phase of matter, *quark-gluon plasma* (QGP)[1, 2].

Quarks and gluons, collectively known as *partons*, are color charged particles those interact via the strong interactions, governed by the theory of Quantum Chromodynamics (QCD). The strong interaction between colored particles weakens asymptotically as the length scale decreases and the energy scale increases, while becoming stronger at larger distance and lower energy, a phenomenon known as the *asymptotic freedom*[3]. Therefore under normal conditions, color charged particles can only exist in "colorless" bound states, for example, protons and neutrons. In contrast, when nuclei collide at ultra-relativistic speed, high temperature and particle density created enables partons to become deconfined, forming the QGP[4].

It is also believed that in the "Big Bang" theory of universe evolution, QGP can be found 20 after the exploration before normal matter forms. Measuring the properties of QGP using "Little Bangs" in the lab can not only provide important insights for the understanding of strong interaction, but also potentially enable us to solidifies our modeling of early universe[5].

1.2 Modeling the QGP as A Nearly Ideal Fluid

Our current understanding of the heavy ion collisions can be roughly devided into the following stages[6]. Starting with the nuclear impact, constituent partons those originally coherently moving coherently along beam direction scatter off each other, obtaining some transverse momentum (p_T) and randomizing. The resulted "state" is commonly known as the *initial conditions*. For most partons, soft scattering happens, meaning relatively low amount of momentum was transferred. This process thermalizes the system, creating the QGP, which then undergoes collective expansion due to internal pressure[7, 8]. As the expansion lower the temperature and density of the medium, particles began to form color neutral bound states of hadrons, which interact with each other, further decay and creates increasing number of particles with decreasing energy as they fly out to surrounding detectors.

It has been proposed as early as in the 1950s that the QGP can be described macroscopically with the Euler equations of motion for an ideal relativistic fluid[9, 7], beginning with thermodynamical fields at initial conditions and ending at "freezing-out" stage. If the QGP has truly behaved accordingly, certain macroscopical features at the initial conditions shall manifest in distributions of final state particles.

One such measurements utilizes the azimuthal anisotropy in final state particles. As shown in Figure 1, the collision geometry of two incoming nuclei vary depending on their directions and impact parameter, introducing a pressure gradient in the initial conditions geometry. As the medium cools down, this gradient leads to a measurable azimuthal anisotropy relative to the reaction plane in final state particles termed *flow*, serving as an important signature for the early stage thermalization of system and sensitive measurements for characterizing the collective expansion[10, 11].

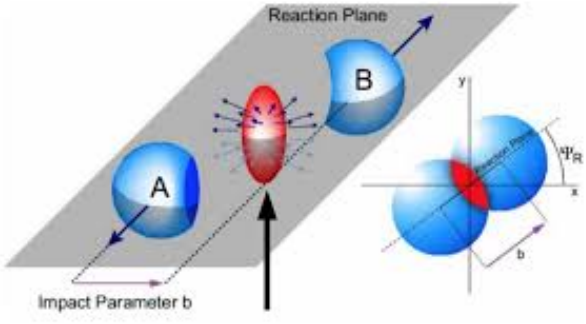

Figure 1: The geometry of nuclei collision[12].

A significant amount of theoretical development and experimental advances has taken place on a quantitative characterization of the QGP, for reviews in better details, see [6, 13, 14]. Here we will discuss some main progresses those are the most relevant for the context of this analysis.

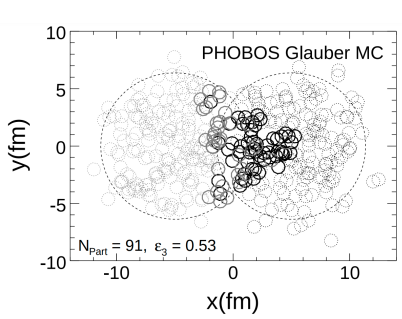

(a) Simulated distribution of nucleons with triangular eccentricity[15].

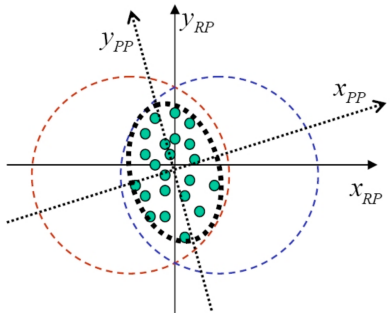

(b) A participant plane (PP) that has an angle with respect to the reaction plane (RP)[9].

Figure 2: Higher flow harmonics and rotated participant plane resulted from nucleon position fluctuations

In 2001, for the first time, experimental data from the Au-Au collisions at 130 and 200 GeV per nucleon-pair at RHIC agreed with predictions using ideal fluid dynamics for collisions with small impact parameters[16]. However, this model gradually diverges from data at larger impact parameters, lower momentum or higher rapidities[17]. It was later theorized that the

transitioning to later hadronic stages needs a microscopic modeling, and a small but non-zero viscosity is required even at the dense QGP state, motivating a series of "hybrid models" those include pre-equilibrium and post-equilibrium treatments in modeling[18, 19]. Another key insight is the role of event-by-event fluctuations in higher order flow harmonics. Event-by-event fluctuations of nucleon positions those participate in collisions creates an initial condition with third and higher order eccentricities those corresponds to higher order flow harmonics, as well as a participant plane that tilts from the reaction plane, as shown in Figure 2. After about 20 years of development since the first confirmation of hydrodynamical model, current models of event-by-event viscous hydrodynamical model has been successful in predicting the translation of initial QGP geometry into final particle v_n for the soft sector[20].

1.3 High p_T Region: A Multilayered Model

On the other hand, the theoretical predictions for flow analysis on the hard sector has been more challenging. These particles are produced from the much rarer hard/semi-hard scatterings during nucleon-nucleon collisions. Two back-to-back travelling parton pairs with large transverse momentum, which travels through the expanding bulk of matter while losing energy through its interaction with the medium. Again, as the system cools down, each parton hadronizes, developing into two highly collimated cones of particles, known as "jets" [8]. When traversing the QGP medium, the partons lose energy to the medium through collisional and induced gluon radiations, "quenching" one of the two back-to-back jets more than the other depending on the propagation length in the medium. The leads to a suppression of high p_T hadrons in heavy ion collisions relative to the nuclear thickness scaling of a proton-proton collision, a quantity measured by the nuclear modification factor R_{AA}[21].

A hydrodynamical description of azimuthal anisotropy is not expected to apply here because the high p_T parton escaped the medium before it can fully thermalized by rescatterings in the medium[17, 7]. Yet since the propagation length in the medium is dependent on azimuthal angle, azimuthal anisotropy is also observed at high p_T region from this parton energy loss inhomogenuity[22]. However, in the past decade, many "jet quenching" models have found it challenging to simultaneously predict for both the R_{AA} and the flow harmonics v_n at high p_T[23, 24, 20, 22]. Resulting from interactions

with an evolving medium, parton energy loss mechanism is also sensitive to the details of the hybrid hydro models that describe the QGP, including its macroscopic parameters, the choice of initial conditions, event-by-event fluctuations, the treatment of pre- and post-equilibrium evolutions and etc[20].

Recent theoretical attempts have tried to incorporate an event-by-event viscous hydrodynamics into a parton energy loss model to solve this puzzle[24, 20]. Different experimentally measured quantities, e.g., R_{AA} and its azimuthal harmonics, v_n and its multi-particle cumulants, probe the same energy loss processes while each being sensitive to different path length dependence and/or hydrodynamical parameters[25]. It is of particular importance to identify a measurable in the statistically challenging high p_T region that allows us to better understand the soft-hard sector correlations, the role of event-by-event fluctuations in the high p_T flow harmonics and thus how flow analysis at high p_T can provide insights for the modeling of the QGP.

2 Experimental Efforts

There're both many existing and ongoing particle detector collaborations at both the LHC and RHIC for flow analysis. Discussed in this section is firstly the upcoming sPHENIX detector at RHIC and then the ATLAS detector at the LHC and its track reconstruction. The second half of this section will be discussing two analysis techniques and each of their focus.

2.1 sPHENIX and the EMCal

The sPHENIX detector at BNL's Relativistic Heavy Ion Collider (RHIC) is an upcoming detector with a calorimeter coverage of $|\eta| < 1.1$ and full azimuth[]. sPHENIX is composed of several sub-detectors, and helping to enable its broad measuring capacity is the electromagnetic calorimeter (EMCal), which is the primary detector for identifying and measuring the energy of photons, electrons, and positrons. The calorimeter blocks of EMCal is constructed of scintillating fibers embedded in blocks of tungsten powder in an epoxy matrix, with a designed angular resolution of 0.25×0.25 in $\eta \times \phi$[]. Two rounds of beam test was done at Fermilab in 2016 and 2018, and with an energy correction strategy developed, the energy resolution of the EMCal prototype was shown to meet the requirements for sPHENIX physics program[26, 27]. The entire EMCal detector is composed of 24576 towers

arranged into 6144 calorimeter blocks, over 5000 of which are being built at the UIUC Nuclear Physics Laboratory. Of crucial importance is the quality assurance (QA) procedure, ranging from the logging of materials to the testing of produced blocks. In 2018-2019, I participated in the EMCal production at UIUC, responsible for improving, automating and coordinating the block testing. Each of the calorimeter blocks is tested for mechanical compliance, density, scintillation performance and fiber percentage, and at planned full production speed, an average of 60 blocks need to be fully tested each week. Therefore, it is important to implement a highly automated, well-documented procedure for student workers to test in an efficient manner with few human errors. For example, for the fiber percentage counting test, I developed a master script where after students have taken the pictures for the tested blocks and copy to the computer, the script will execute sub-routines, each of which reads the block ID from the picture, crops the relevant region, count the number of fibers, organize the picture into local destinations and cloud back-up, and upload analysed results to a shared spreadsheets where all blocks' production and testing information is located. Shown on Figure. **??** is the testing workflow and shown on Figure. **??** is an example fiber counting image. The EMCal production at UIUC up to 2021, March has produced 46% of required blocks.

2.2 ATLAS

2.2.1 The LHC

The Large Hadron Collider (LHC) underground beneath the France Switzserland border near Geneva is the world's largest and highest-energy particle collider built by the European Organization for Nuclear Research (CERN). Installed in a circular 26.7 km tunnel, the LHC consists of two rings with counter-rotating beams of particles, such as proton-proton or heavy ion collisions like xenon-xenon, lead-lead or proton-lead, etc. Four detector facilities can be found at four points on the ring where the two beams cross, and they are, A Toroidal LHC Apparatus (ATLAS), Compact Muon Solenoid (CMS), A Large Ion Collider Experiment (ALICE) and Large Hadron Collider beauty (LHCb)[28]. Achieving its first collision at 2010, the LHC has then been operating and then upgraded, with Run 1 taking data between 2009-2013, and Run 2 between 2015-2018. And now the LHC is being further upgraded with the goal of implementing the High-Luminosity Large Hadron Collider

(HL-LHC).

2.2.2 ATLAS Detector

The ATLAS detector is a multipurpose particle detector installed at the LHC covering a nearly full azimuthal range and large pseodorapidity[1]. Thus it is well suited for our proposed analysis to explore correlations of particles over large angular range[30, 29]. A diagram of ATLAS sub-detectors is shown in Figure **??**. The proposed analysis will rely on the inner detectors, the calorimeters and the data acquisition and trigger system.

The calorimeter system measures energy deposit made by particles as they interact with and lose energy to the detectors. Electromagnetic calorimeters measure the energy of electrons and photons, surrounded by the hadronic calorimeters which sample the energy of hadrons, such as protons and neutrons. The sampling calorimeters have barrel and end-cap parts, covering the range $|\eta| < 4.9$ to provide with energy and position information for interaction products and spectator particles[30]. The Zero-Degree calorimeters also detect neutral particles for pseudorapidity range $|\eta| > 8.3$ and trigger for collisions with very large impact parameters[31].

The tracking detectors, also known as the inner detectors (ID), is responsible for measure the trajectories and momentum of charged particles within $|\eta| < 2.5$[30]. Located closest to the interaction point, the tracking system comprises of three subsystems of cylindrically coaxial layers that are immersed in a 2 T axial magnetic field. Shown on Figure **??** is the structure diagram for ID, going from innermost outward are the silicon pixel detectors, silicon microstrip detectors (SCT), and a straw-tube transition-radiation detector (TRT). An additional pixel detector "insertable B-layer" (IBL) was installed as the innermost layer for Run 2 to improve tracking performance as well as mitigating radiation damage from higher luminisities[32]. Hits from inner detectors are clustered using a set of devoted algorithms into objects termed *tracks*, representing the measured charged particle with vertex,

[1]ATLAS uses a right-handed coordinate system with origin located at the nominal interaction point (IP). Its positive x-aixs points toward the center of the LHC ring, positive y-axis points upward against and thus defining a positive z-axis along beam direction. In analysis related to angular directions, a cylindrical system (r, θ) is defined in the x-y plane, or the *transverse plane*. The beam direction angle is usually expressed in pseudorapidity $\eta = -\ln \tan(\theta/2)$, where θ is the polar angle. The measurement of two objects' angular separation is expressed in terms of $\Delta R = \sqrt{(\Delta\eta)^2 + (\Delta\phi)^2}$ between the two objects[29].

direction, momentum, charge, and etc.

The counter-rotating beams of particles at LHC consists of trains of bunches which collide when two bunches cross, and each collision is called an *event*. The nominal interval between the passage of successive bunches is 25 ns. At the designed luminosity of $10^{-34} cm^{-2} s^{-1}$, proton-proton interactions is at approximately 1 GHz, while data recording is limited to the rate of about 200 Hz. Therefore, the trigger and data acquisition (TDAQ) systems of ATLAS is needed to selectively trigger and process events of interest[30]. The ATLAS trigger system consists of a fast hardware level-1 (L1) trigger based on electronics and programmable logic, and high-level triggers (HLT) with lower frequency that's based on software algorithms. A prescale factor can also be applied to only sample a proportion of all triggered events to further reduce data size. Multiple trigger systems exist to sample over different phase space of data, for example, tracks from the minimum-bias (MB) triggered events are mainly low p_T while jet-triggers can extend to higher p_T. Data from different triggers are merged in such a way that the resulting spectrum is equivalent to an unbiased spectrum. Shown on Figure **??** is the comparison of the merged sample to MB samples[**?**]. To obtain more data for specific analysis need, Partial Event Building (PEB) technique is also used, where only certain detector information, for example, tracks only, is saved. During Run 2, heavy ion data has been taken for PbPb collisions at an average center of mass energy per nucleon pair $\sqrt{s_{NN}} = 5.02$ TeV, with an intergrated recorded luminosity of 548 ub^{-1} in 2015 and 1.76 nb^{-1} in 2018. While full events are saved for part of minimum bias triggers and some triggers of rarer selections, charged particle trajectories, or *tracks* as will be discussed below, are saved for nearly full MB triggers un-prescaled, providing with rich resources for analysis using charged particles.

3 Analysis Techniques

3.1 Key Ingredients

3.1.1 Event Centrality

The event centrality is a measurement of impact parameter for two colliding nuclei. In ATLAS, it is measured by the total energy deposited ΣE_T in the forward calorimeter (FCal), which covers pseudorapidity range $3.2 < |\eta| < 4.9$. It is defined as a percentile of ΣE_T distribution, starting at 0% for

the most central collisions, where two nuclei collide each other head-on, and larger percentage for more peripheral collisions with larger impact parameter.

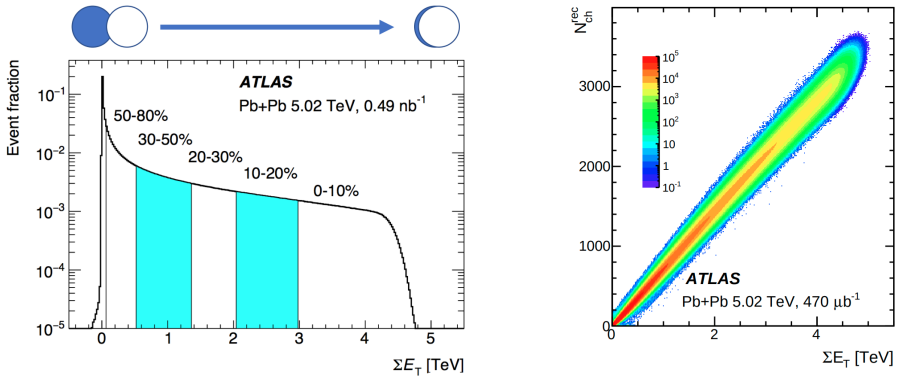

(a) ΣE_T distribution for Pb+Pb data at 5.02 TeV with centrality labelled.

(b) The number of reconstructed charged particles per event at different centrality[29].

Figure 3: Centrality division and event multiplicity using Pb+Pb.

To provide with information for each centrality range, a Monte Carlo Glauber simulation is matched to the Pb+Pb events. These simulations contain only the hadronic fraction of Pb+Pb cross section, defined as events those went through at least short-distance hadronical interaction between one pair of nucleons, one from each nucleus. These events are said to be Glauber-like, and their geometrica quantities, such as number of participant nucleon N_{part}, number of binary nucleon-nucleon collision N_{coll} are obtained from the Glauber simulation for each centrality range. For Run 2 Pb+Pb data obtained by ATLAS, about 85% of total mimimum bias events are matched to the Glauber simulation. The ΣE_T cut values are determined from distribution of data. The minimum bias Pb+Pb events from Run 2 are sorted by their ΣE_T values and divided into 85 bins of equal sizes, corresponding to the 85% Glauber-like event fraction. These cuts account for detector and collision energy conditions that's specific for Run 2 Pb+Pb data measured at ATLAS[29]. Shown in Figure 3a is the ΣE_T correspondence with centrality, and Figure 3b shows how number of reconstructed charged particles in events are correlated with centrality[29].

The particle production spectra reflected in the nuclear modification factor R_{AA} and azimuthal modulation is centrality dependent due to different

event multiplicity and rates of hard scattering. R_{AA} is a ratio of yields per nucleon-nucleon interactions in heavy ion system relative to the *pp* collisions. Due to parton energy loss, the production of charged hadrons are suppressed. Shown in Figure **??** is the measurement of R_{AA} by ATLAS at $\sqrt{s_{NN}} = 5.02$ TeV for Pb+Pb data, and as expected the suppression is the most significant at central events. Since high p_T flow harmonics are also theorized to rise from parton energy loss, anisotropy in R_{AA} can be used as probe for high p_T flow calculations[24, 20].

3.1.2 Tracks and Jets Reconstruction

Charged particles are measured by the inner detectors in ATLAS as *tracks*, in ATLAS, the minimum p_T of reconstructed tracks in the Pb+Pb samples is 0.5 GeV. The occupancy of particles produced in HI collisions is highly centrality dependent, creating difference in the reconstruction performance for different centrality. Tracks reconstructed can be graded into 14 different quality classes, based on the availability of hits from all layers of ID, whether the hits are shared by other reconstructed tracks, etc.[33]. The reconstructed tracks are also used to fit the primary interaction vertex (PV) in each event using the vertex finding and fitting algorithm, and only one primary vertex is considered in heavy ion events. Each track is calculated the momentum and emitting direction in terms of (η, ϕ), as well as impact parameters $z_0 \sin\theta$ and d_0 in longitudinal and transverse direction, measured with respect to the primary vertex at the point of closest approach, helping determining whether they come from primary interaction or secondary decays as particles travel out from the collision.

Jets in ATLAS heavy ion collisions are reconstructed from energy deposit in calorimeter towers with the $anti - k_T$ algorithm[34]. In this algorithm, soft particles are iteratively clustered into a cone with nearby hard particles to form jets with a given radius R. Firstly, a list of energy deposits objects E_i in calorimeter towers with angular resolution $\eta \times \phi = 0.1 \times 0.1$ are obtained. For each pair of two objects i and j, two "distances" that characterize both their energy and spatial separation relations are defined and compared: $d_{i,j} = \min(E_i^(-2), E_j^(-2)) \frac{\Delta_{i,j}^2}{R^2}$ and $d_{i,B} = E_i^{-2}$ where B signifies with respect to *beam*. If $d_{i,j} < d_{i,B}$, the two objects merges into one new object at their energy weighted average position. If $d_{i,B} < d_{i,j}$, then the object is considered a jet with radius R and removed from the list. This process iterates until the list is cleared. Since hard particles have larger E_i thus smaller $d_{i,j}$ for neigh-

boring particles, soft particles are more likely to cluster around hard ones to form jets before they cluster amongst themselves, therefore constructing jets those are dominated by hard particle positions.

3.1.3 Jet Flavour Tagging Using Tracks

Flavour tagging is the identification of jets containing b or c hadrons. A set of algorithms exploiting quantities like decay time and multiplicity of $b-$ and $c-$ jets are developed in pp analysis to identify $b-$ and $c-$ jets from light jets, using profiles of physics variables extracted from tracks associated to jets. However, these algorithms have not been optimized for heavy ion events, which have a higher occupancy and more *underlying events* (UE), the detector measurements of particles from soft interactions. More tracks that are not related to jets are used by the algorithm, modifying the variables and interfering with tagging.

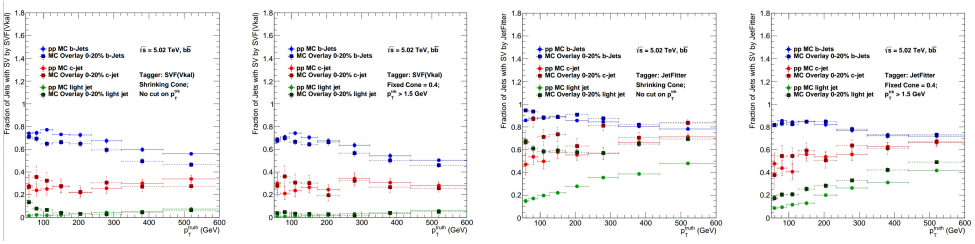

(a) (b) (c) (d)

Figure 4: The comparison of secondary vertexing performance using two taggers. 4a4b show results with SVF tagger, and 4c4d show the JetFitter tagger. 4a4c shows results with the shrinking cone track-to-jet association and no requirements on track minimum p_T, and the second row shows results with fixed cone at $R = 0.4$ and tracks with $p_T > 1.5$ GeV.

For my ATLAS authorship qualification task, I studies strategies to optimize the flavour tagging in heavy ion environment. One approach is to improve the performance of secondary vertex (SV) reconstruction using tracks. SV are reconstructed vertex where heavy flavour hadrons decay. Due to different track distribution in jets between PbPb and pp jets, I found that the spatial proximity based track-to-jet association algorithm "shrinking cone" was tuned based on pp simulations, thus excluding useful tracks for PbPb

samples where track in jets distribution is different, reducing vertexing efficiency especially for SVF tagger as shown in Figure 4a. On the other hand, since UE tracks are dominantly low p_T, the high fake rate as shown in Figure 4c can be decreased by choosing a higher p_T cut on tracks. The combination of these two strategies are shown to improve secondary vertexing efficiency without introducing significant additional fake rate, as shown in 4b4d. Another approach is to remake the physics variable templates, such as impact parameters, with PbPb simulations in a certain centrality bin and tag using templates from the same centrality. As shown in Figure 5, the tagging ROC curve using remade templates are improved for central heavy ion events and has a weaker centrality dependence.

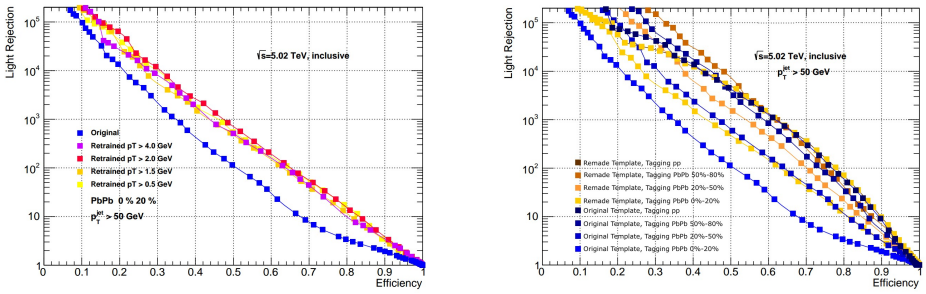

Figure 5: ROC cruve for tagging using IP3D, the impact parameter tagger, with *pp* template and templates remade from *PbPb* simulations with different p_T selections. Shown curve is tagging results for the most central heavy ion events.

3.2 Analysis Technique

To compare with the n-th order eccentricities of initial geometry, the invariant yield of particle azimuthal distributions measured with respect to the reaction plane at angle Ψ_{RP}can be characterized by a Fourier expansion,

$$E\frac{d^3N}{dp^3} = \frac{1}{2\pi}\frac{d^2N}{p_t dp_t dy}(1 + \sum_{n=1}^{\infty} 2v_n \cos[n(\phi - \Psi_{RP})]) \tag{1}$$

where E and ϕ is the energy and azimuthal angle of particle, y is the rapidity, and $v_n = \langle \cos[n(\phi_i - \Psi_{RP})] \rangle$ is known as the n-th order flow harmonics[35], where the brackets $\langle\rangle$ denotes average overall particles of all events. v_1 is

known as the directed flow, the elliptical geometry of the QGP as the one shown in Figure.1 will give raise to a second-order flow harmonics v_2, and v_3 corresponds to a triangular flow and so on. v_n is a function of p_T and rapidity, thus termed the n-th order *differential* flow[9]. Using the kinematic relationship $\tanh(y) = \frac{p_z}{E}$ and a cylindrical coordinate to transform the invariant yield,

$$\frac{d^3N}{dp^3} = \frac{d^3N}{p_t dp_t dp_z d\phi} = \frac{d^2N}{p_t dp_t dp_z}\frac{dN}{d\phi} = \frac{d^N}{Ep_t dp_t dy}\frac{dN}{d\phi} \tag{2}$$

giving the integrated particle azimuthal distribution,

$$\frac{dN}{d\phi} = \frac{1}{2\pi}(1 + \sum_{n=1}^{\infty} 2v_n \cos[n(\phi - \Psi_{RP}]) \tag{3}$$

The reaction plane cannot be measured directly in experiments but instead, an observed *event plane* is reconstructed from using produced particles themselves. For each harmonic mode n, a weighted event flow vector $\mathbf{Q_n}$ is defined as,

$$\mathbf{Q_n} = (\sum_j w_j \cos(n\phi_j), \sum_j w_j \sin(n\phi_j)) = (\cos(n\Psi_n), \sin(n\Psi_n)) \tag{4}$$

and therefore $\Psi_n = \tan^{-1}(\frac{Q_{n,y}}{Q_{n,x}})$. This defines the basics of the *standard event plane method*[36]. However, the measured event plane is subjected to detector acceptance defects and non-flow correlations of particles, for example, particles of the same jet. Two methods are discussed below those aim to strengthen the flow signals and suppress non-flow effects.

3.2.1 scalar product method

The scalar product extends from the standard event plane method by utilizing the length of flow vector as weight when taking average over the events, which maximizes the measured flow values and is shown to reduce statistical uncertainties[37]. The v_n coefficient can be expressed with,

$$v_n\{\text{SP}\} \equiv \frac{\langle Q_n Q^*_{n,A}\rangle}{\sqrt{\langle Q_{n,A} Q^*_{n,B}\rangle}} \tag{5}$$

where $Q_{n,A}$ and $Q_{n,B}$ is the Q-vector magnitude using two identical subevents. The numerator in equation (5) gives the regular v_n expression while

the denominator corrects for measurement resolution of event plane. Dividing a full event into two or multiple sub-events can separate event plane resolution for different detector section, and more over enable we impose pseudo-rapidity gap when correlating particles from different sub-events and suppress short-range non-flow correlations. In actual experiments where identical sub-events are unavailable, three sub-events can be used substituting the denominator with $\sqrt{\frac{\langle Q_{n,A}Q^*_{n,B}\rangle\langle Q_{n,A}Q^*_{n,C}\rangle}{\langle Q_{n,B}Q^*_{n,C}\rangle}}$[38, 23]

3.2.2 multi-particle cumulant method

The scalar product method is still sensitive to few particle correlations, motivating for the use of higher order multi-particle cumulants[39]. For example, four correlations are not sensitive to two-particles' non-flow correlations, and since contributions like resonance decays scale with $\frac{1}{M^3}$, where M is the particle multiplicity, "direct" four-particle correlations are much rarer. The basic principle for multi-particle cumulants attempts to decompose a many particle correlation, for example, correlations between all particles in an event, into a series of sum involving correlations between smaller number of particles. In the standard cumulant method[35, 29], The event-average azimuthal correlations for an event with multiplicity M between two- and four-particle is defined as,

$$\langle\langle 2\rangle\rangle \equiv \langle\langle e^{in(\phi_1-\phi_2)}\rangle\rangle = \frac{\sum_i^{events}(W_{(2)})_i\langle 2\rangle_i}{\sum_i^{events}(W_{(2)})_i} \tag{6}$$

$$\langle\langle 4\rangle\rangle \equiv \langle\langle e^{in(\phi_1+\phi_2-\phi_3-\phi_4)}\rangle\rangle = \frac{\sum_i^{events}(W_{(4)})_i\langle 2\rangle_i}{\sum_i^{events}(W_{(4)})_i} \tag{7}$$

where $\langle n\rangle_i$ is the single-event averaged n-particle correlations for event i. The second order cumulant $c_n\{2\}$ is defined as,

$$c_n\{2\} \equiv \langle\langle e^{in(\phi_1-\phi_2)}\rangle\rangle - \langle e^{in\phi_1}\rangle\langle e^{-in\phi_2}\rangle = \langle\langle 2\rangle\rangle - \langle\langle 1\rangle\rangle^2 \tag{8}$$

And the second term vanishes when detector acceptance is uniform. For uniform detectors, the fourth-order cumulant $c_n\{4\}$ is defined as,

$$c_n\{4\} = \langle\langle 4\rangle\rangle - 2\langle\langle 2\rangle\rangle^2 \tag{9}$$

These cumulants are averaged over all particles in an event, and they reflect the integrated flow terms in relations,

$$\begin{aligned} c_n\{2\} &= \langle\langle v_n^2 \rangle\rangle, \\ c_n\{4\} &= \langle\langle v_n^4 \rangle\rangle - 2\langle\langle v_n^2 \rangle\rangle^2 \end{aligned} \tag{10}$$

It can be seen that flow harmonics $v_n\{k\}$ extracted from k-th order cumulant has different sensitivity to the event-by-event fluctuations. In the following section, a specific quantity using multi-particle cumulants is derived to specifically probe event-by-event fluctuations in high p_T flow and soft-hard correlations.

3.3 Soft-hard particle Correlation in Cumulant Framework

The experimental measurement of p_T dependent differential flow harmonics $v_n(p_T)$ in high p_T region is usually carried out utilizing a correlation between an integrated flow vector of soft region and p_T dependent target hard particles. In the event plane method and its variants, the event plane angle is dominated by soft particles[24, 20]. In the cumulant framework, the multi-particle correlation differential in p_T is calculated with only the particle of interest restricted to a p_T range. The single-event average correlation is denoted as $\langle k' \rangle$ for k-particle correlation. The differential cumulants $d_n\{2\}(p_T)$ and $d_n\{4\}(p_T)$ and different flow $v_n\{4\}(p_T)$ and $v_n\{4\}(p_T)$ are derived from Ref. [39, 35] for a detector of uniform acceptance to be,

$$\begin{aligned} d_n\{2\}(p_T) &= \langle\langle 2' \rangle\rangle, \\ d_n\{4\}(p_T) &= \langle\langle 4' \rangle\rangle - 2\langle\langle 2' \rangle\rangle\langle\langle 2 \rangle\rangle \end{aligned} \tag{11}$$

$$\begin{aligned} v_n\{2\}(p_T) &= \frac{d_n\{2\}(p_T)}{(c_n\{2\})^{1/2}}, \\ v_n\{4\}(p_T) &= \frac{d_n\{4\}(p_T)}{(-c_n\{4\})^{3/4}} \end{aligned} \tag{12}$$

The event-averaged differential correlators $\langle\langle k' \rangle\rangle$ can be computed with equation (6) and (7) by replacing $\langle k \rangle$ with its differential variant $\langle k' \rangle$. An event weight is chosen to minimize the effect of event multiplicity. Experimentally, the event weight W_i is the number of different k-particle combinations in that event[35]. In modeling, multiplicity M_i is used for soft particles while $R_{AA}(p_T)$ that reflects nuclear particle yield is used for hard particle[20].

4 Proposed Research

The low p_T flow harmonics analysis have been measured by collaborations at LHC and RHIC with different techniques and collision energy, the results of which helped constraining parameters, such as initial conditions, bulk and shear viscosity, etc. Modeling based on event-by-event viscous relativistic hydrodynamic has shown impressive simultaneous predictions for integrated and differential multiple v_n at different centrality, with further tuning possible to improve predictions of peripheral events. For example, a hybrid model IP-Glasma+MUSIC+UrQMD, using fluctuating initial conditions viscous hydrodynamics with microscopic framework for hadronic cascade process. As shown in Figure 6a for event plane method and Figure 6b for multi-particle correlations, the prediction achieved overall good agreement with measurements at both LHC and RHIC systems, with deviations in peripheral events, especially for the event plane method, potentially from the residual non-flow effects or better tuning of fluid transport parameters. Since peripheral events have lower multiplicity as shown in Figure 3b, few particle correlations are more profound in peripheral events. The fluctuations at low p_T can also be well-estimated using initial eccentricities fluctuations as shown in Figure 6c[40].

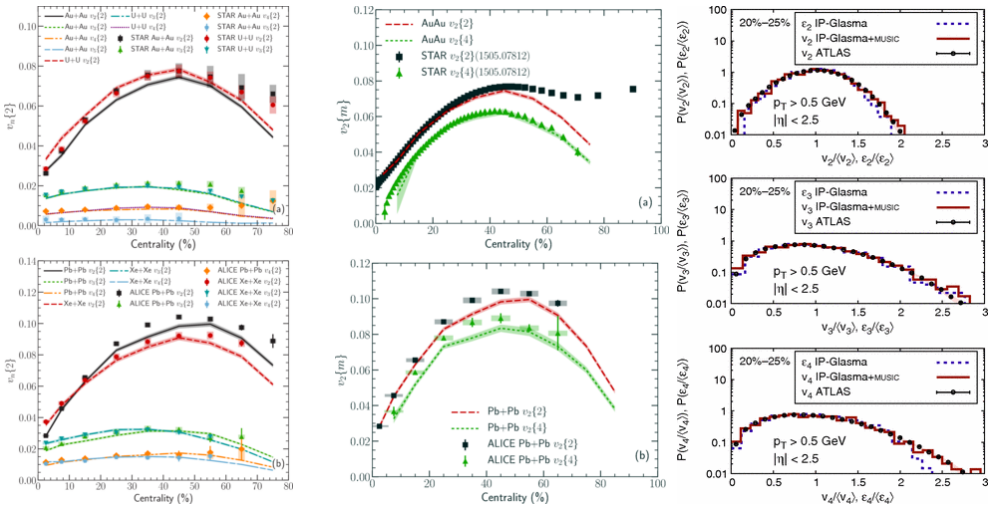

(a) Comparison for event plane method.

(b) Comparison for multi-particle cumulant method.

(c) Matching soft v_n distribution to ϵ_n.

Figure 6: Low p_T flow harmonics measured at LHC and RHIC compared to hybrid viscous hydrodynamical model IP-Glasma+MUSIC+UrQMD[41], and distribution of $v_n/\langle v_n\rangle$ measured at LHC comparing to $\epsilon_n/\langle\epsilon_n\rangle$ using IP-Glasma+MUSIC[40].

As discussed in section 1.3, the modeling of high p_T particle production suggested the combination of event-by-event hydrodynamics with a parton energy loss model, the parameters of both can be contraint by different experimental variables. Techniques for measuring the flow harmonics are also devised, with the utilization of hard-soft correlations for measuring high p_T flow harmonics where statistics are limited. The measurements of high p_T flow harmonics, especially through its p_T dependent cumulants, each of which have different sensitivity to local particle correlations, can show whether the behavior of high p_T flow harmonics is consistent with a collective expanding medium[23].

We propose to measure the high p_T differential flow using multi-particle cumulant methods with charged particles from ATLAS Pb+Pb data. A measurement of v_n will be firstly measured with the scalar product methods, and two- and four- particle cumulants with sub-event methods with imposed η gap to suppress nonflow effect. We specifically propose to measure the multi-particle cumulant ratios to reveal important information about how

response to initial state geometry differs with p_T. It has been shown in Ref [20] that, if the fluctuations of high p_T v_2 were correlated to the soft fluctuations exactly in a linear manner, then, $v_2\{4\}(p_T)/v_2\{2\}(p_T) = v_2\{4\}/v_2\{2\}$ for all p_T. Similarly, the deviation of the differential cumulant ratio from its integrated counterpart will constrain the p_T dependence of response to fluctuations in initial geometry. The calculations for $v_2\{4\}(p_T)/v_2\{2\}(p_T)$ using LHC condition for $\sqrt{s_{NN}} = 5.02$ Tev PbPb collision are available for comparison[20].

Integrated and differential flow measurements with ATLAS have been done with pp, pPb, and PbPb systems at low p_t. More importantly, hard-soft correlations using high p_T jet flow measurements in PbPb has been measured in $\sqrt{s_{NN}} = 2.67$ TeV and $\sqrt{s_{NN}} = 5.02$ GeV, as shown in Figure 7a, and high p_T v_2 in PbPb has also been measured with multi-particle correlation by the CMS collaboration as shown in Figure **??**. The same detector measurements with different system size and methods will provide references and better constraints for modeling.

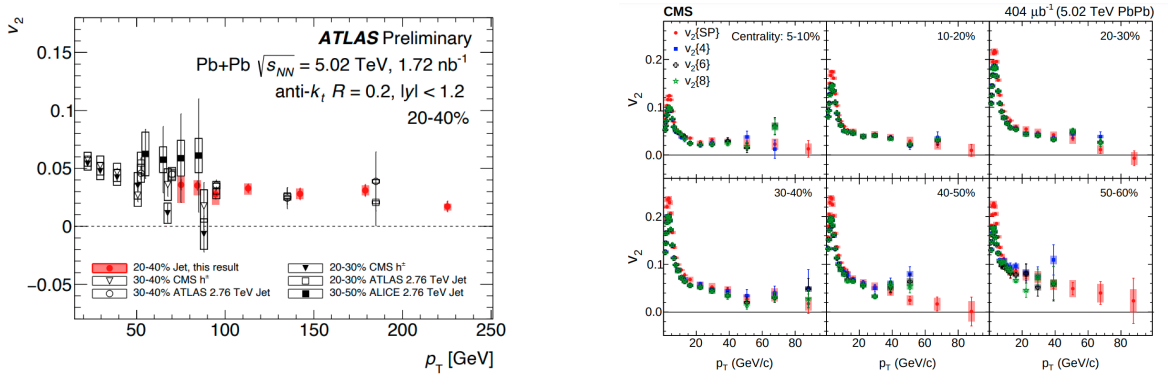

(a) (b)

Figure 7: Hard-soft correlation measurements from LHC data using, (left)jet correlating with event plane, and (right)multi-particle cumulants and scalar product method[42, 23].

We propose to measure the differential flow harmonics up to 100 GeV with the 470 μb^{-2} of $\sqrt{s_{NN}} = 5.02$ TeV data collected by ATLAS in 2015. Firstly, the performance of tracks should be evaluated, including the momentum resolution of tracks, trigger efficiency and track reconstruction efficiency. This should take approximately 3 months. Then, correction strategies and

nonflow suppresion methods should be developed, exploiting techniques developed by previous ATLAS and other LHC flow measurements for the fake track rejection, detector azimuthal nonuniformity correction and sub-event methods. The completion of these corrections will prepare for a preliminary measurements and uncertainty evaluation, and we plan to have this preliminary result by the spring of 2022, with the rest of 2022 for finalization of measurements.

References

[1] Edward V. Shuryak. Quantum chromodynamics and the theory of superdense matter. *Physics Reports*, 61(2):71–158, 1980.

[2] Roman Pasechnik and Michal Šumbera. Phenomenological Review on Quark–Gluon Plasma: Concepts vs. Observations. *Universe*, 3(1):7, 2017.

[3] J. C. Collins and M. J. Perry. Superdense matter: Neutrons or asymptotically free quarks? *Phys. Rev. Lett.*, 34:1353–1356, May 1975.

[4] Mark Thomson. *Modern particle physics*. Cambridge University Press, New York, 2013.

[5] Johann Rafelski. Melting hadrons, boiling quarks. 2015.

[6] Ulrich W Heinz and Raimond Snellings. Collective flow and viscosity in relativistic heavy-ion collisions. 2013.

[7] Peter F. Kolb and Ulrich Heinz. Hydrodynamic description of ultrarelativistic heavy-ion collisions, 2003.

[8] Wit Busza, Krishna Rajagopal, and Wilke van der Schee. Heavy ion collisions: The big picture, and the big questions. 2018.

[9] Sergei A. Voloshin, Arthur M. Poskanzer, and Raimond Snellings. Collective phenomena in non-central nuclear collisions. *Landolt-Bornstein*, 23:293–333, 2010.

[10] A. M. Poskanzer and S. A. Voloshin. Methods for analyzing anisotropic flow in relativistic nuclear collisions. *Phys. Rev. C*, 58:1671–1678, Sep 1998.

[11] Xin-Nian Wang. Jet quenching and azimuthal anisotropy of large p_t spectra in non-central high-energy heavy-ion collisions. 2000.

[12] M. Stefaniaka H.Zbroszczyk. Examination of the heavy-ion collisions using epos model in the frame of bes program at rhic. In *Proc. of 5th International Conference on New Frontiers in Physics*, EPJ Web Conf., page 8. EDP Sciences, 2017.

[13] Roman Pasechnik and Michal Šumbera. Phenomenological review on quark-gluon plasma: Concepts vs. observations. 2016.

[14] Rafael Derradi de Souza, Tomoi Koide, and Takeshi Kodama. Hydrodynamic approaches in relativistic heavy ion reactions. 2015.

[15] B. Alver and G. Roland. Collision geometry fluctuations and triangular flow in heavy-ion collisions. 2010.

[16] Ulrich W. Heinz and Peter F. Kolb. Early thermalization at rhic. 2001.

[17] Ulrich W. Heinz. Hydrodynamics at RHIC - How well does it work, where and how does it break down? *J. Phys. G*, 31:S717–S724, 2005.

[18] Hannah Petersen. Anisotropic flow in transport+hydrodynamics hybrid approaches. 2014.

[19] Matthew Luzum and Paul Romatschke. Conformal relativistic viscous hydrodynamics: Applications to rhic results at sqrt($s_n n$) = $200 gev$.2008.

[20] Jacquelyn Noronha-Hostler, Barbara Betz, Miklos Gyulassy, Matthew Luzum, Jorge Noronha, Israel Portillo, and Claudia Ratti. Cumulants and nonlinear response of high p_t harmonic flow at $\sqrt{s_{NN}} = 5.02$ tev. 2016.

[21] Ivan Vitev and Miklos Gyulassy. High p_T tomography of d + Au and Au+Au at SPS, RHIC, and LHC. *Phys. Rev. Lett.*, 89:252301, 2002.

[22] ATLAS Collaboration. Transverse momentum and process dependent azimuthal anisotropies in $\sqrt{s_{\mathrm{NN}}} = 8.16$ tev p+pb collisions with the atlas detector. 2019.

[23] CMS Collaboration. Azimuthal anisotropy of charged particles with transverse momentum up to 100 gev in pbpb collisions at sqrt(s[nn]) = 5.02 tev. 2017.

[24] Jacquelyn Noronha-Hostler, Barbara Betz, Jorge Noronha, and Miklos Gyulassy. Event-by-event hydrodynamics + jet energy loss: A solution to the $r_{AA} \otimes v_2$ puzzle. 2016.

[25] Jiangyong Jia, W. A. Horowitz, and Jinfeng Liao. A study of the correlations between jet quenching observables at rhic. 2010.

[26] C. A. Aidala et. al. Design and beam test results for the sphenix electromagnetic and hadronic calorimeter prototypes. 2017.

[27] C. A. Aidala et al. Design and Beam Test Results for the 2D Projective sPHENIX Electromagnetic Calorimeter Prototype. *IEEE Trans. Nucl. Sci.*, 68(2):173–181, 2021.

[28] LHC Machine. *JINST*, 3:S08001, 2008.

[29] Sven Reichardt and Ludger Wirtz. Non-adiabatic exciton-phonon coupling in raman spectroscopy of layered materials. 2019.

[30] The ATLAS Collaboration et.al. The ATLAS experiment at the CERN large hadron collider. *Journal of Instrumentation*, 3(08):S08003–S08003, aug 2008.

[31] Marco A. L. Leite. Performance of the ATLAS Zero Degree Calorimeter. In *2013 IEEE Nuclear Science Symposium and Medical Imaging Conference and Workshop on Room-Temperature Semiconductor Detectors*, 2013.

[32] M. Capeans, G. Darbo, K. Einsweiler, M. Elsing, T. Flick, M. Garcia-Sciveres, C. Gemme, H. Pernegger, O. Rohne, and R. Vuillermet. ATLAS Insertable B-Layer Technical Design Report. 9 2010.

[33] ATLAS Collaboration. Measurement of charged-particle spectra in pb+pb collisions at $\sqrt{s_{\mathsf{NN}}} = 2.76$ tev with the atlas detector at the lhc. 2015.

[34] Matteo Cacciari, Gavin P. Salam, and Gregory Soyez. The anti-$\mathrm{k}_t jet clustering algorithm$. 2008.

[35] Ante Bilandzic, Raimond Snellings, and Sergei Voloshin. Flow analysis with cumulants: Direct calculations. *Phys. Rev. C*, 83:044913, 2011.

[36] A. M. Poskanzer and S. A. Voloshin. Methods for analyzing anisotropic flow in relativistic nuclear collisions. 1998.

[37] STAR collaboration. Elliptic flow from two- and four-particle correlations in au + au collisions at sqrts$_{NN} = 130gev.2002$.

[38] Matthew Luzum and Jean-Yves Ollitrault. Eliminating experimental bias in anisotropic-flow measurements of high-energy nuclear collisions. 2012.

[39] Nicolas Borghini, Phuong Mai Dinh, and Jean-Yves Ollitrault. Flow analysis from multiparticle azimuthal correlations. 2001.

[40] Charles Gale, Sangyong Jeon, Björn Schenke, Prithwish Tribedy, and Raju Venugopalan. Event-by-event anisotropic flow in heavy-ion collisions from combined Yang-Mills and viscous fluid dynamics. *Phys. Rev. Lett.*, 110(1):012302, 2013.

[41] Bjoern Schenke, Chun Shen, and Prithwish Tribedy. Running the gamut of high energy nuclear collisions. *Phys. Rev. C*, 102(4):044905, 2020.

[42] Measurements of Jet Azimuthal Anisotropies in Pb+Pb collisions at $\sqrt{s_{NN}}$ = 5.02 TeV. 6 2020.

integrated cumulant measurements at low pt https://arxiv.org/pdf/1904.04808.pdf
CMS measurements, scalar product method + differential cumulants https://arxiv.org/pdf/1702.00
direct calculation of differential cumulants https://journals.aps.org/prc/pdf/10.1103/PhysRevC.83.

5 Key Quantities Defined

5.1 jets

5.2 track reconstruction(?)

5.3 flow harmonics

5.4 multiparticle cumulants

6 proposed research

A differential multiparticle cumulant measurements using ATLAS 5.02 TeV PbPb data A measurements of the integrated multiparticle cumulants are done for particles with pT ¡ 10 GeV https://arxiv.org/pdf/1904.04808.pdf

Probing into modeling high pt flow using soft-hard flow correlation requires a differential cumulants measurements instead.

1. performance evaluation. (might need trigger efficiency) https://cds.cern.ch/record/2702964/f
COM-PHYS-2019-1424.pdf?version=14 2. evaluate differential vn with scalar product method (used almost everywhere)(equivalent to event plane) template fitting + two-particle correlation http://cdsweb.cern.ch/record/2318870/files/ATLAS-CONF-2018-011.pdf(XeXe differential in pt up to 15 GeV) (don't do this) citations: https://arxiv.org/pdf/1509.04776.pdf (pp 13/2.76 TeV ATLAS) https://arxiv.org/pdf/1609.06213.pdf (pp + pPb 2PC 5.02 TeV ATLAS) https://arxiv.org/pdf/1910.13978.pdf (pPb 8.16 ATLAS) recommended by Anne (not done above 20 GeV) 3. evaluate differential cn with direct calculation: https://journals.aps.org/prc/pdf/10.1103/PhysRevC.83.044913 (CMS method https://arxiv.org/pdf/1702.00630.pdf + ATLAS PbPb: https://arxiv.org/pdf/1904.04808.

subevent method: https://arxiv.org/pdf/1701.03830.pdf differential flow can be done similarly

only cumulants ratio + SP method flow high pt 2PC is not feasible above 20 GeV with data 4. unfolding systematics (only one paper from above mentioned unfolding, and it's only referencing to a CMS result)